Two Particle Interferometry at RHIC

F. Laue[a] for the STAR Collaboration*

[a]The Ohio State University

We present preliminary results from a pion interferometry analysis of Au+Au Collisions at $\sqrt{s_{NN}} = 130$ GeV, recorded with the STAR (**S**olenoidal **T**racker **A**t **R**HIC) detector at the **R**elativistic **H**eavy **I**on **C**ollider (RHIC). The evaluation of three-dimensional correlation functions indicates increasing source sizes with increasing event centrality. The dependence of the calculated HBT radii on transverse momentum is attributed to strong space-momentum correlations (transverse flow). In the study presented in this paper we have not observed anomalously large source sizes as have been predicted as a signal for quark-qluon plasma formation. However, the measured HBT radii seem to follow the trend established at lower energies (AGS/SPS). We find the ratio $R_o/R_s \approx 1$, suggesting a short duration of pion emission. The "universal" pion phase space density, observed at AGS/SPS, seems to hold also at RHIC.

1. Introduction

Intensity interferometry, originally invented by Hanbury-Brown & Twiss for stellar size determination[1], is nowadays a commonly-used tool to study heavy ion collisions. The primary goal of an HBT analysis, performed at mid-rapidity and low transverse momentum, is to study the spatio-temporal size of the particle emitting source. However, it also contains information about the emission pattern in momentum space (e.g. radial flow) which can be explored by studying the HBT parameters as a function of transverse momentum[2].

Experimentally, the two-particle correlation function is obtained as $C_2(\mathbf{q}) = A(\mathbf{q})/B(\mathbf{q})$. Here $A(\mathbf{q})$ is the measured distribution of the momentum difference $\mathbf{q} = \mathbf{p_1} - \mathbf{p_2}$ calculated using particles from the same event, and $B(\mathbf{q})$ is the corresponding distribution calculated from particles from different events. Throughout this paper, we will refer to $A(\mathbf{q})$ as the *same event distribution*, we will refer to $B(\mathbf{q})$ as *mixed-event background distribution*. Quantum interference gives a rise to a an enhancement in $C(\mathbf{q})$ for $q < \hbar/R$, where R is the source size[1].

2. The Experimental Setup and Data Sample

The data we report on was taken with the STAR Time Projection Chamber (TPC)[3], the main tracking device of the STAR experiment. The TPC is placed in a solenoidal magnet which was operated at a 0.25 Tesla field, allowing tracking of particles with

*for a complete author list please see [21] transverse momenta $p_T > 75$ MeV/c. For this study we have restricted the kinematic region $|y| < 0.5$, $0.125 \leq p_T/(\mathrm{GeV/c}) \leq 0.45$, for which particle identification and the momentum resolution, $\Delta p/p \leq 2\%$, is optimum.

2.1. Event Selection

For each event, the primary vertex was calculated from the many tracks originating from the collision. The primary vertices were distributed over about 0.5 mm in the transverse directions (x, y) and over more than a meter along beam direction (z). To assure that this wide vertex z-position does not distort the single particle phase space and acceptance on an event by event basis, we restricted our analysis to events located within ± 75 cm, measured from the center of the 4 m long TPC. Furthermore, we mixed events only if their longitudinal primary vertex positions were not farther apart than 15 cm. We divided our data Sample into 3 centrality classes where centrality was defined by the number of negatively charged tracks in one unit of pseudo-rapidity at mid-rapidity ($|\eta| < 0.5$). Each centrality bin contains more than 10^5 events and constitutes approximately the top 12%, $12\% - 32\%$ and $32\% - 72\%$ most central events.

2.2. Particle Selection

We selected particles in the three transverse momentum intervals $0.125 < p_T/(\mathrm{GeV/c}) < 0.225$, $0.225 < p_T/(\mathrm{GeV/c}) < 0.325$ and $0.325 < p_T/(\mathrm{GeV/c}) < 0.45$, leading to mean transverse pair-momenta of $\langle p_T \rangle \approx 0.17$ GeV/c, $\langle p_T \rangle \approx 0.27$ GeV/c and $\langle p_T \rangle \approx 0.38$ GeV/c, respectively. All tracks were required to point back to the primary vertex within 3 cm and to consist of at least 10 hits, 45 being the maximum number of hits defined by the TPC's 45 padrows per sector. Particle identification was achieved by correlating the magnetic rigidity of a track with its specific ionisation (dE/dx) in the gas of the TPC. Pions can easily be separated from kaons and protons within the applied kinematic cuts(see Fig. 4 in[4]). The main contribution of non-pions to our data sample are electrons which fall in the relativistic rise of the energy loss distribution for the momentum range in question. We estimated that the contamination of electrons is below 10% (4%) for our lowest (highest) p_T interval. Electrons as well as pions from resonance decays that can not be rejected by the 3 cm vertex cut lead to an overall reduction of the strength of the correlation function. This will be seen in a reduced λ factor, leaving the extracted HBT radii unchanged [5,6].

2.3. Pair Selection

Well known problems to particle interferometry analyses in TPCs are track-splitting[2] and track-merging[3]. While the estimated fraction of split or merged tracks is less than 1% for the STAR data, this may have strong effects on the correlation function. Track-merging leads to a loss of low-q pairs while the combination of two same-track-fragments results in a rise of the correlation function at low q.

To reject pairs from split tracks we used a cut based on the hit pattern of the two tracks on the TPC's padrows. False pairs generated by track-splitting are removed by a topological cut which requires valid and distinct signals of both tracks on several TPC padrows.

---

[2] a track from a single particle is misidentified by the reconstruction software as two or more tracks
[3] two tracks being close together in the TPC volume are misidentified as a single particle

To eliminate track-merging effects in the TPC, we require the tracks in a pair to be well separated (> 2.5 cm at the radius of the TPC inner field cage, 50 cm). In applying this cut to the mixed-pair background distribution, the effect of the event-to-event variation in primary vertex position is taken into account. This anti-merging cut– while necessary to remove detector effects– itself affects the correlation function by discriminating mostly against low-q pairs, which carry the correlation signal. This leads to an artificial reduction in the HBT parameters, which we estimated, based on simulations, to be 3-6% for the radii and 6-14% for λ, depending on p_T. In the results presented here, we remove this artificial reduction in the parameters.

2.4. The Analysis

Applying the cuts mentioned above, we calculated the correlation functions, weighting each background pair with a Coulomb correction as it is standard in HBT analyses. As the Coulomb correction we used a 5-dimensional Monte-Carlo integration of Coulomb wave functions over a spherical source [7,8]. This correction is identical to the one used by other experiments at lower energies [5,9,8]. The upper left panel (a) of Fig. 1 shows the Coulomb–corrected and uncorrected 1-dimensional $\pi^-\pi^-$ correlation $C(Q_{inv})$ as a function of the Lorentz–invariant variable $Q_{inv} = \sqrt{(\mathbf{p_1} + \mathbf{p_2})^2 - (E_1 + E_2)^2}$ for our highest multiplicity bin and for our lowest p_T cut. Here, the Coulomb correction was applied for a 5 fm source and a Gaussian fit of the form $C(Q_{inv}) = 1 + \lambda e^{(-Q_{inv}^2 R_{inv}^2)}$ applied to the corrected data. The fit clearly underestimates the correlation at low Q_{inv}, as observed in previous measurements [10], and the extracted radius $R_{inv} = (6.29 \pm 0.11)$ fm only indicates roughly the source size.

The panels (b)-(d) of Fig. 1 show projections of the multi-dimensional correlation function $C(q_o, q_s, q_l)$ in the Pratt-Bertsch parameterisation for the same data sample. Here, the relative momentum $\mathbf{q}$ was measured in the Longitudinally Co-Moving Source (LCMS) frame, in which the total momentum of the pair in beam direction vanishes, and is decomposed in the 3 components q_o, q_s, q_l[4] according to [7,11]. Again, the Coulomb correction was done assuming a 5 fm source and a (3-dimensional) Gaussian fit was $C(q_o, q_s, q_l) = 1 + \lambda e^{-q_o^2 R_o^2 - q_s^2 R_s^2 - q_l^2 R_l^2}$ applied. The fit is shown as lines in Fig. 1 and was weighted with the mixed-event background to reflect the measured phase space.

The incoherency parameter λ which measures the strength of the correlation is determined as $\lambda \approx 0.5$, implying that only 1/2 of the accepted pairs represent pairs of pions directly from the collisions region. In this case, the procedure of applying the Coulomb correction to *every* background pair may be questioned. As shown in Fig. 2(right panel), Coulomb–correcting only 1/2 of the background pairs leads to an increase in R_o and R_l of $\approx 10\%$, with little effect on R_s. Also shown is the influence of assuming different source sizes for the Coulomb correction on the HBT radii which is also of about 10%, when varying $R_{Coulomb}$ within reasonable parameters between 4–8 fm.

In the following, however, we corrected all background pairs using a 5 fm Coulomb-source for better comparison with lower energy data [5,10,13] and calculated the Pratt-Bertsch parameters for our three centrality bin and three transverse momentum bins.

[4] q_{long} is the relative momentum component parallel to the beam axis, q_{out} along the pair transverse momentum and q_{side} the component perpendicular to q_{long} and q_{out},for brevity we replace *out, side, long* subscripts with *o,s,l* in the text

Systematic errors on the HBT fit parameters, indicated by the shaded bands in Fig. 3, arise from roughly equal contributions of two sources: (1) the uncertainty on the removal of the artificial reduction associated with the anti-merging cut is estimated to be equal with the reduction itself, and (2) varying the radius in the Coulomb correction by ± 1 fm, which induces a small variation (0.1-0.2 fm) in the HBT radii. We did not apply a momentum-resolution correction yet, which is estimated to be a 10% correction on the radii for our highest momentum bin. Systematic uncertainties from other sources are negligible.

3. Results and Discussion

3.1. Pion HBT

Fig. 3 (left panels) presents the multiplicity dependence of the source parameters for pions at low p_T and mid-rapidity. The parameters are very similar for positively and negatively charged pions. While λ stays constant, all radii increase with increasing multiplicity. For R_o and R_s this increase is attributed to the geometrical overlap of the two nuclei and was also observed at lower energies [5,12,13]. An increase in R_l, however, was not observed at lower energies. The right panels of Fig. 3 shows the dependence of the HBT parameters on transverse mass, m_T, for our highest multiplicity bin. Here, λ increases slightly with m_T, which can be understood as a decreasing contribution of pions from long-lived resonances. All the extracted radii rapidly decrease as a function of m_T, and our results hereby differs in from SPS energies, where the observed decrease in R_o is not as strong[14].This strong decrease of the radius parameters may be due to strong transverse flow[15].

While for transparent sources the emission duration is given by $\tau = \sqrt{R_o^2 - R_s^2}/\beta_T$, we measure $R_o/R_s < 1$ at higher transverse momenta which might be an indication of opaqueness of the source[16,17] and/or an explosive[18] source. We clearly do not observe $R_o/R_s \gg 1$ as a predicted signature due to the onset of QGP formation [19,20]. However, [20] also states that this signature vanishes again, once the energy is well above the onset, further motivating a systematic scan from SPS energies (corresponds to RHIC injection energy) up to full RHIC energies.

Compiling our findings and results from lower energies we plot the $\pi^-\pi^-$ HBT excitation function (see Fig.17 in [21] for central heavy ion collisions at low p_T and mid-rapidity. Our data point for λ follows the systematic established at AGS and SPS, starting off at unity and falling to $\lambda \approx 0.5$ with increasing energy as expected from stronger contributions of pions from long-lived resonances. While R_o stays more or less constant over the whole energy range, R_s and R_l have an initial decrease at AGS energies, attributed to increasing space-momentum correlations[5]. Somewhere between AGS and SPS R_o and R_l start to rise again, reflecting a larger freeze-out volume due to increasing pion multiplicity. Our data points nicely extend this trend.

3.2. The Pion Phase space Density

Combining the HBT radii from this analysis and the π^- momentum distribution $\frac{d^2N}{dydm_T}$ [21] allows us to extract the 6-dimensional pion phase space density, i.e., the average number of pions per phase space cell of the volume $\hbar^3$[22]. The pion phase space density

(PSD) is of great interest, because it allows to determine important source characteristics such as the freeze-out temperature and average flow velocity. We calculated the PSD as

$$\langle f \rangle (m_T) = \frac{(\hbar c)^2}{2E_\pi m_T} \frac{d^2N}{dy dm_T} \frac{(\lambda \pi)^{1/2}}{R_o R_s R_l} \qquad (E_\pi \text{ is the total pion energy}). \tag{1}$$

The values we extracted are shown in Fig. 4 together with values from SPS energies, indicating that the "universal" phase space distribution observed at SPS and AGS[23] also holds at RHIC energies. Also shown are fits to a Bose-Einstein distribution (solid lines) and to a modified Bose-Einstein distribution taking transverse flow in account (dashed lines) according to [24]. Here, a linear dependence of λ and a power-law like scaling of the HBT radii with m_T is assumed, so that the PSD can be extrapolated to $p_T = 0$ MeV/c, where the transverse flow vanishes. This leads to a freeze-out temperature of $T_0 = (94.3 \pm 0.6)\ MeV$ and with an effective temperature of $T_{eff} = 185\ MeV$[21] (measured as the inverse slope parameter of the π^- m_T-distribution) the average transverse flow velocity can be calculated as $\beta_T = (T_{eff}^2 - T_0^2)/(T_{eff}^2 + T_0^2) = 0.58 \pm 0.018$, consistent with the velocity of sound as predicted by relativistic hydrodynamics, $\beta_{sound} = 1/\sqrt{3} = 0.577$. Note, elliptical flow measurements at RHIC also coincide with hydrodynamics calculations[25,26].

4. Conclusion

We have performed the first pion interferometry measurements at RHIC energies and hereby extended the HBT excitation function into the new energy domain. We do not observe extraordinarily large radii of the pion emitting source, but our observations follow the systematics established at lower energies.

All the Pratt-Bertsch HBT radii increase with event multiplicity, while $\lambda \approx 0.5$ stays constant. As a function of transverse mass, m_T, all the extracted radii rapidly decrease, indicating strong transverse flow. λ increases with m_T, suggesting a smaller contribution of pions from long-lived decays.

The ratio $R_o/R_s \approx 1$ may indicate a short duration of pion emission. However, it should be noted that the effects of strong transverse flow and a possible opaque source on the R_o/R_s ratio have to be studied in greater detail. It would be interesting to perform a systematic scan over the whole energy range available at RHIC to clearly search for jumps in the lifetime which might happen only in a relative small energy range.

The *"universal"* pion phase space density as measured at AGS and SPS seems to hold also at RHIC. The transverse flow velocity extracted in our new phase space density measurement at RHIC is consistent with relativistic hydrodynamics predictions.

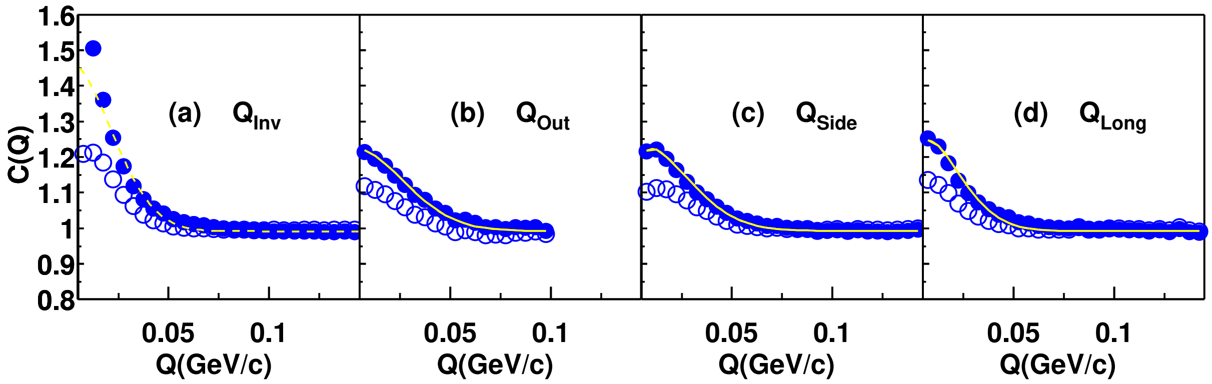

Figure 1. Coulomb–corrected (full symbols) and uncorrected (open symbols) $\pi^-\pi^-$ correlation functions for high multiplicity events at mid-rapidity ($|y| < 0.5$) and low transverse momentum ($0.125 < p_T/(GeV/c) < 0.225$) from Au+Au–Collisions at $\sqrt{s_{NN}} = 130 GeV$. Panel (a) shows the 1-dimensional correlation function. $C(Q_{inv})$. The Panels (b)-(d) show projections of the 3-dimensional correlation functions $C(q_o, q_s, q_l)$ on the q_o, q_s and q_l axis, respectively. For each projection the correlation function is integrated over the range 0–20 MeV/c for the other two components. The lines represent the 1-dimensional(a) and 3-dimensional (b)-(d) fit of a Gaussian distribution to the Coulomb–corrected data.

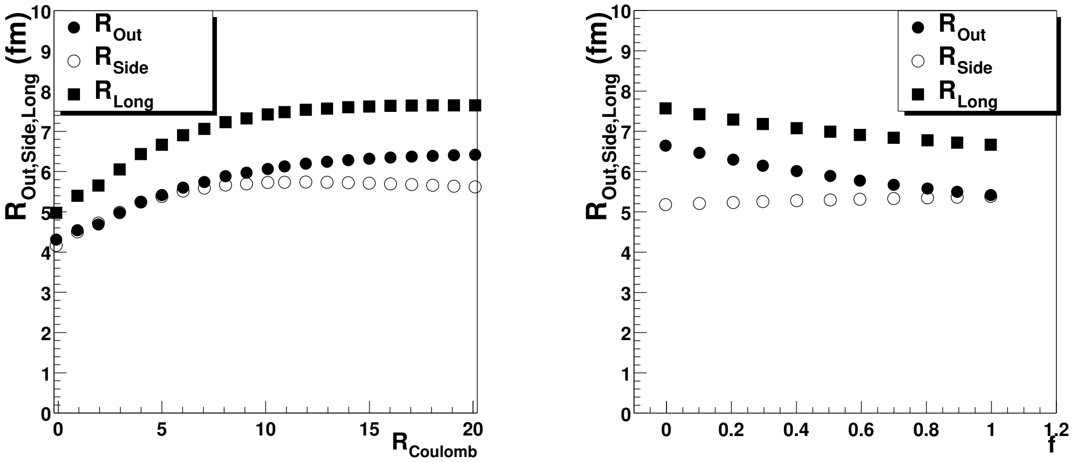

Figure 2. Left panel: Extracted HBT radii as a function of the Coulomb source size $R_{Coulomb}$. Right panel: Extracted HBT radii as a function of the fraction of Coulomb-corrected background pairs f ($f = 0$ means no Coulomb correction, $f = 1$ means full standard Coulomb correction).

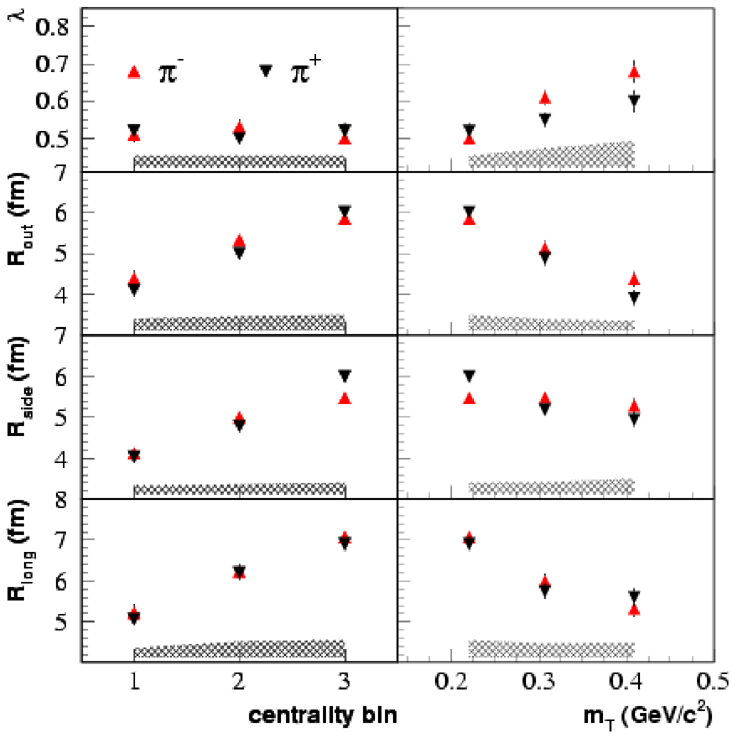

Figure 3. Multiplicity and m_T-dependence of the $\pi^{\pm}\pi^{\pm}$ HBT parameters. Left, multiplicity dependence: The data shown represents our low p_T bin (p_T = 0.125–0.225 GeV/c). Right, m_T-dependence: The data is shown for our highest multiplicity bin. The error bars indicate the statistical uncertainties only, the shaded bands reflect the systematic uncertainties.

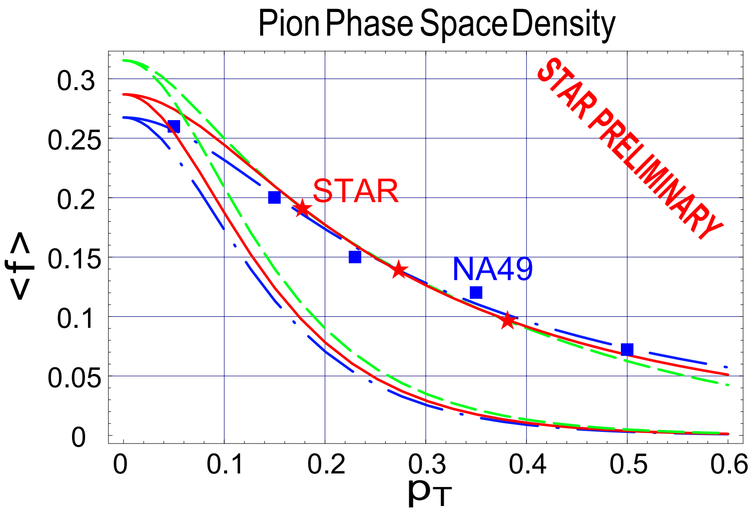

Figure 4. Comparison of pion phase space density $\langle f \rangle$ at the SPS and RHIC: Square symbols are NA49 results for $Pb + Pb$ at $\sqrt{s_{NN}}$ = 18 GeV and the star symbols are STAR results (preliminary) for Au+Au at $\sqrt{s_{NN}} = 130$ GeV. The upper curves show $\langle f \rangle$ derived from a fit to the STAR HBT radii (dashed) and the Bose-Einstein $\langle f \rangle$ distributions including transverse flow in a linearised Tomasik model[24], with freeze-out temperatures of 94.3 MeV (solid) derived from a fit to the STAR results and 89.7 MeV (dash-dot) derived from a fit to the NA49 results. The lower curves show for comparison the Bose-Einstein $\langle f \rangle$ distributions assuming no transverse flow for freeze-out temperatures of 99.5 MeV (dashed), 94.3 MeV (solid), and 89.7 MeV (dash-dot). Note that flow and no-flow BE $\langle f \rangle$ values coincide at $p_T = 0$.

REFERENCES

1. R. Hanbury Brown, R.Q. Twiss., Phil.Mag.45(1954)663
2. W. Bauer *et al.*, Ann. Rev. Nucl. Part. Sci. 42(1992)77; U. Heinz and B. Jacak, Ann. Rev. Nucl. Part. Sci. 49(1999)529; U.A. Wiedemann and U. Heinz, Phys. Rep. 319(1984)1219;
3. K.H. Ackermann *et al.* (STAR Collaboration), Nucl.Phys.A661(1999)681
4. F. Retiere *et al.* (STAR Collaboration), Proceedings of this conference
5. M. Lisa *et al.* (E895 Collaboration), Phys. Rev. Lett. 84, 2789(2000)
6. H. Appelshäuser (NA49 Collaboration), Ph.D. Thesis, University of Frankfurt (1996)
7. S. Pratt *et al.*, Phys. Rev. C42(1990)2646
8. J. Barrette *et al.* (E877), Nucl. Phys. A610(1996)227; J. Barrette *et al.*, Phys. Rev. Lett. 78(1997)2916
9. K. Kadija *et al.* (NA49 Collaboration), Nucl. Phys. A610(1996)248
10. I.G. Bearden *et al.* (NA44 Collaboration), Phys. Rev. C58, 1656(1998)
11. G. Bertsch *et al.*, Phys. Rev. C37(1988)1896
12. R. Soltz *et al.* Nucl. Phys. A611(1999)439
13. R. Ganz *et al.* (NA49 Collaboration), Nucl. Phys. A661(1999)450
14. C. Blume (NA49 Collaboration), Proceedings of this conference
15. B. Tomasik *et al.*, Nucl.Phys.A663(2000)753
16. Eur. Phys. J. C1(1998)593; Phys. Lett. B421(1998)18
17. B. Tomasik and U Heinz *et al.*, nucl-th/9805016
18. A. Dumitru and R. Pisarski*et al.*, hep-ph/0102020
19. D. Rischke, Nucl.Phys.A610(1996)88
20. D. Rischke and M. Gyulassy, Nucl.Phys.A608(1996)479
21. J. Harris (STAR Collaboration), Proceedings of this conference
22. G. Bertsch *et al.*, Phys. Rev. Lett. 72(1994)2349
23. D. Ferenc, Phys. Lett. B457(1999)347
24. B. Tomasik, Ph.D. Thesis, University of Regensburg (1999)
25. R. Snellings (STAR Collaboration), Proceedings of this conference
26. K.H. Ackermann *et al.* (STAR Collaboration), Phys.Rev.Lett.86(2001)402